Strengthening and Toughening of a Heavy Plate Steel for Shipbuilding with Yield Strength of Approximately 690 MPa

DONGSHENG LIU, BINGGUI CHENG, and YUANYUAN CHEN

HSLA-100 steel with high content of alloying elements (nominally in wt pct, 3.5 Ni, 1.6 Cu, and 0.6Mo) is now used to produce heavy plates for constructing a hull and drilling platform. We proposed here a substantially leaner steel composition (containing 1.7 Ni, 1.1 Cu, and 0.5Mo) to produce a heavy plate to 80 mm thickness with mechanical properties comparable with those of the HSLA-100 grade. A continuous cooling transformation (CCT) diagram of the steel was constructed. Key parameters of thermal treatment and revealing mechanisms of strengthening and toughening were derived based on industrial production trials. The microstructures of the 80-mm-thick plate were lath-like bainite (LB) at near surface of the quarter thickness ($t/4$), and granular bainite (GB) + LB at center thickness ($t/2$) after solutionizing and water quenching (Q). The effect of tempering (T) on the microstructures and properties of the plate was investigated. Excellent combination of room temperature strength and low-temperature Charpy V-notch (CVN) toughness approximately equivalent to that of the HSLA 100 grade (YS > 690 MPa, CVN energy >100 J even at 193 K [−80 °C]) was achieved in the plate treated by the QT process with tempering temperature of 898 K (625 °C). The combination of strength and toughness at $t/4$ is superior to that at $t/2$ of the plate under both as-quenched and QT conditions. This result is attributed to that the fraction of high-angle grain boundaries (HAGBs) at $t/4$ is higher than that at $t/2$.

I. INTRODUCTION

ADVANCED heavy steel plates with ultrahigh strengths, enhanced low-temperature toughness, and improved weldability are widely used for shipbuilding, bridge, pressure vessels, and offshore structures. The low-carbon copper-bearing HSLA-100 plate steel developed three decades ago is an excellent example for producing the advanced plates with minimum yield strength (YS) of 690 MPa to meet the demands of the above applications.[1–8] The great significance of using HSLA-100 steel plates for ship hull construction is that the preheating step can be eliminated to reduce the time cost of welding. However, high contents of expensive alloying elements (nominally in wt pct, 3.35-3.65Ni, 1.45-1.75Cu, 0.55-0.65Mo, and 0.45-0.75Cr, *etc*.) are added in the steel.[4] Solutionizing (austenitizing), water quenching, and tempering (QT) process steps following hot rolling are required to achieve the target mechanical properties. The final microstructure consists of tempered lath-like martensite (LM) containing ε-Cu precipitates with newly formed interlath retained austenite even in a 51-mm-thick plate.[9] The previous studies, however, were all restricted to the plates no thicker than 51 mm.[4–9]

To construct larger ships and drilling platforms for efficient transportation and energy exploration in remote cold areas, highly ductile, heavy steel plates thicker than 50 mm are required. The production of such advanced steel plates with the strength and toughness levels equivalent to those of the HSLA-100 with reduced contents of Ni and Cu is significant to maximize the economy of both steel company and shipbuilder. Laboratory trials were conducted on a lean steel composition compared with that of the HSLA-100 steel with substantial reductions in Ni and Cu. The results indicated that balanced strength and toughness equivalent to that of the HSLA-100 steel can be obtained in the water-quenched steel plates after tempering at 923 K (650 °C) for 60 minutes.[10]

Any production specifications made based on laboratory results cannot be directly applied into commercialization until these are tested and preferably verified by industrial production trials. This was employed here. For industrial production, the challenge is to produce YS 690 class heavy-thickness (*e.g.*, up to 80 mm) steel plates with good combination of strength and low-temperature toughness across the entire thickness section when the maximum continuously cast (CC) slab thickness and mill configuration are limited. For that, advanced heat-treatment technology following the production of clean steel and homogenous slab,[11] modern thermomechanical rolling, and accelerated cooling is essential.[12,13]

The variation of as-quenched microstructures depending on the cooling rate, quenching temperature, and steel composition has a significant influence on the

DONGSHENG LIU, Senior Researcher and Manager, and BINGGUI CHENG and YUANYUAN CHEN, Assistant Researchers, are with the Institute of Research of Iron and Steel, Shasteel, Jinfeng, Zhangjiagang, Jiangsu 215625, People's Republic of China. Contact e-mail: dongsliu@gmail.com

mechanical properties of the plates. Dhua *et al.*[9] studied the effect of as-quenched microstructure on mechanical properties of HSLA-100 plates. They found that the plates with full LM exhibited balanced tensile strength and low-temperature toughness. The plates with granular bainite (GB) exhibited substantially decreased tensile strength and poor Charpy V notch (CVN) impact toughness. The influence of tempering on the mechanical properties of Cu-bearing YS 690 MPa class heavy steel plates with as-quenched microstructure of LM has been extensively investigated.[1–6] However, the study on tempering response of the YS 690 MPa Cu bearing steel plates with range of bainitic microstructures has received less attention.

In the current work, a low-carbon MnCrMoNiCu steel slab with much lower Ni and Cu concentrations than those of HSLA-100 steel was thermomechanically rolled into a heavy plate to 80 mm thickness, solutionized, and water quenched. The variations of the microstructural factors and mechanical properties on tempering have been investigated together with continuous cooling transformation (CCT) behavior of austenite. Microstructures of the plate were characterized with optical microscope (OM), scanning electron microscope (SEM), transmission electron microscope (TEM), and electron backscatter diffraction (EBSD) techniques. A good combination of strength and low-temperature toughness [YS > 690 MPa, CVN toughness >100 J even at 193 K (-80 °C)] has been achieved in the 80-mm-thick plate, which is well above the specification defined by Det Norske Veritas for NV-F690 ship steel.

II. EXPERIMENTAL

The chemical composition of the subject steel is characterized by low carbon content (0.07 wt. pct) with balanced additions of alloy elements (manganese, chromium, nickel, copper, and molybdenum) and microalloying elements (niobium and titanium), as shown in Table I. Carbon equivalent of 0.64 and P_{cm} value of approximately 0.27 were chosen to maximize weldability. Slabs of 320 mm thickness were produced by an integrated industrial-production system described elsewhere.[14]

According to solubility equation employed by Mousava Anijdan and Yue[15] taking the effects of Mn and Si concentrations into account, it was estimated that the solution temperature of Nb(C,N) is 1397 K (1124 °C) for the current steel. After soaking at 1473 K (1200 °C) for 120 minutes where Nb(C,N) is fully in solution, one of the slabs was subjected to descaling, rough rolling, delay, finish rolling to 80 mm thickness, lamellar water flow cooling, hot leveling, and ultrasonic detection. Two-stage rolling, *i.e.*, rough rolling and finish rolling, were conducted at austenite recrystallization region and nonrecrystallization region with predetermined rough rolling reduction ratio (RR) and finish rolling reduction ratio (FR). Key thermomechanical controlled processing (TMCP) parameters for the rolled plate including the total RR and FR, finish rolling entry temperature (T_{in}) and exit temperature (T_{out}), accelerated cooling (AcC) rate (ϕ), and AcC finish temperature (T_{FC}) are listed in Table II. All the recorded temperatures were measured on the plate top surface.

Austenite decomposition kinetics during CCT was studied by dilatometric technique with a Gleeble 3800 thermomechanical simulator (Dynamic System Inc., Poestenkill, NY). Shouldered round tensile samples for the CCT measurements were sectioned from the TMCP processed plate and tested as described previously.[14,16] When the cooling rates were at 50 K/s to 200 K/s (50 °C/s to 200 °C/s), samples with the geometry used by Colla *et al.*[17] were used and water was pumped through the hollow shoulders on both ends to achieve the desired cooling rates in the midspans of the samples.

The 80-mm-thick plate was then subjected to solutionizing at 1168 K (895 °C) for 170 minutes, and water quenching in the heat-treatment shop equipped with a roll quenching machine. Accurate measurements of the cooling rates of quenching were not conducted during the industrial production process. It is, however, estimated according to the data achieved during hot commissioning that the maximum cooling rate at the core of the heavy plate to 80 mm thickness is 5 K/s (5 °C/s) at temperature range below 1073 K (800 °C). Then, 80-mm-thick blocks suitable for evaluating the mechanical properties were sectioned from the as-quenched plate. These were then tempered in an air furnace at temperatures varying from 673 K to 948 K

Table I. Chemical Composition of the Investigated Steel (Weight Percent)

C	Si	Mn	P	S	Al	Nb	Ti	Cr	Cu	Ni	Mo	N ppm
0.07	0.21	1.03	0.008	0.002	0.036	0.042	0.014	0.60	1.08	1.68	0.47	31

Table II. Processing Parameters Employed during the Industrial Rolling

Thickness t (mm)	Rough Rolling		Finish Rolling		Accelerated Cooling		
	T_{RR} [K (°C)]	RR (pct)	T_{in} to T_{out} [K (°C)]	FR (pct)	ϕ K/s (°C/s)	T_{SC} [K (°C)]	T_{FC} [K (°C)]
80.0	1313 to 1223 (1040 to 950)	50.0	1113 to 1127 (840 to 854)	50.0	10 (10)	1123 (850)	783 (510)

(400 °C to 675 °C) for 240 minutes followed by water quenching.

Tensile properties and CVN impact properties in the transverse direction (TD) at center thickness ($t/2$) and quarter thickness ($t/4$) were tested. Round-shouldered samples with 8 mm gauge diameter and 50 mm gauge length were machined from the subplates. The tensile samples were tested at room temperature using a crosshead speed of 5 mm/min on a tensile machine (model Instron 5585; Instron Corp., Canton, MA) with 250-kN capacity. The YS was measured at the 0.2 pct offset stress. CVN impact tests were performed on standard samples (size: $10 \times 10 \times 55$ mm) with the V notch parallel to the normal direction (ND) at 213 K to 193 K (-60 °C to -80 °C) employing a 450-J instrumented pendulum impact tester (model IMP450J Dynatup; Instron) with a tup striker radius of 2 mm.

To investigate the microstructure and properties of the heat-affected zone (HAZ) of the weld, rectangular specimens of $10 \times 10 \times 75$ mm were made from the 80-mm-thick plate in the central 10-mm section of the plate. The HAZ simulations were performed using the Gleeble 3800 thermomechanical simulator (Dynamic Systems, Inc.) employing the Rykalin-3D (thick plate) heat-transfer model.[8] A Pt-10 pct Rh thermocouple was spot welded at the central length of a specimen for recording the temperature. The specimen was heated at 180 K/s to 1623 K (180 °C/s to 1350 °C) (T_P^1), held for 1 second, and cooled down at the cooling rate ($\Delta t_{8/3}$, i.e., the time from 1073 K to 773 K (800 °C to 300 °C)) ranging from 38 to 62 seconds. The peak temperature of the second thermal cycle (T_P^2) was varied between 873 K and 1473 K (600 °C and 1200 °C) for simulating the thermal cycle due to the second weld bead. CVN specimens were made with the notch at the central length, i.e., the spot-welded thermocouple position along the original ND-RD orientation of the plates, and the CVN impact energy was measured at 213 K (-60 °C).

Polished specimens along ND-RD orientation at $t/2$ and $t/4$ were examined by etching in a 4 vol pct nital solution and observed with an optical microscope and a field-emission SEM (FEI's model Quanta 3D FEG; FEI Corporation, Hillsboro, OR). EBSD analysis (resolution: 0.2 μm) was conducted employing a field-emission SEM (model: JSM-7001F; JEOL Ltd., Tokyo, Japan) equipped with an EBSD camera. The data were then interpreted by Channel 5 software (HKL Technology A/S, Hobro, Denmark). For the CCT samples, the central plane perpendicular to the length direction was examined. These samples were also subjected to Vickers microhardness measurement employing a Tukon 2100B tester (Instron Corporation) using a 10-kg load. A more detailed metallographic examination was performed on selected specimens using a TEM (model: JEM-2100F; JEOL Ltd.) equipped with energy-dispersive spectrometry attachment. Thin foils for TEM were prepared in a twin-jet electrolytic apparatus using a solution containing 5 vol pct perchloric acid and 95 vol pct ethanol, and they were examined at 200 kV.

III. RESULTS

A. Thermomechanical Simulation: CCT Diagram, Microstructure, and Hardness

The CCT tests were conducted from austenite microstructures formed by austenitizing at 1168 K (895 °C) and isothermal holding for 5 minutes. The average austenite grain size prior to continuous cooling transformation was approximately 10 μm, which was observed by a Confocal scanning microscopy employing the procedures described elsewhere.[14] Nonlinear cooling curves were achieved for the samples cooled at rates higher than 5 K/s (5 °C/s) at temperatures lower than 723 K (450 °C). Figure 1 depicts the CCT diagram of the subject steel. Representative SEM micrographs of the Gleeble specimens cooled at rates from 0.25 K/s to 200 K/s (0.25 °C/s to 200 °C/s) are shown in Figure 2. The A_{c1} and A_{c3} temperatures that were measured during continuous heating at 5 K/s (5 °C/s) were 973 K and 1113 K (700 °C and 840 °C). Polygonal ferrite transformation was not observed within the cooling rate range. Bainite transformation started at 813 K (540 °C) and ended at 643 K (370 °C) at 0.25 K/s (0.25 °C/s) and 2.5 K/s (2.5 °C/s) resulting predominantly GB. Coarse martensite-austenite (MA) constituents sized at 2 μm were observed at 0.25 K/s (0.25 °C/s). The size of the MA decreased to 0.5 μm as the cooling rate increased to 2.5 K/s (2.5 °C/s). Full lath-like bainite (LB) with fine MA constituents between the laths was produced when the cooling rates were greater than 10 K/s (10 °C/s), while full LM was obtained at cooling rates higher than 50 K/s (50 °C/s) with martensite transformation starting at 713 K (440 °C). The hardness values increased gradually with the cooling rate, reaching the highest HVN of 365 for the LM microstructure.

The CCT behavior of the current steel is compared with those of the HSLA-80 (nominally in wt pct, 0.05C, 0.5Mn, 1.12Cu, 0.88Ni, 0.71Cr, and 0.20Mo) and HSLA-100 steels.[9,18] The microstructure of the HSLA-80 steel cooled at 10 K/s (10 °C/s) consists mainly polygonal ferrite (PF) + Widmanstätten ferrite,
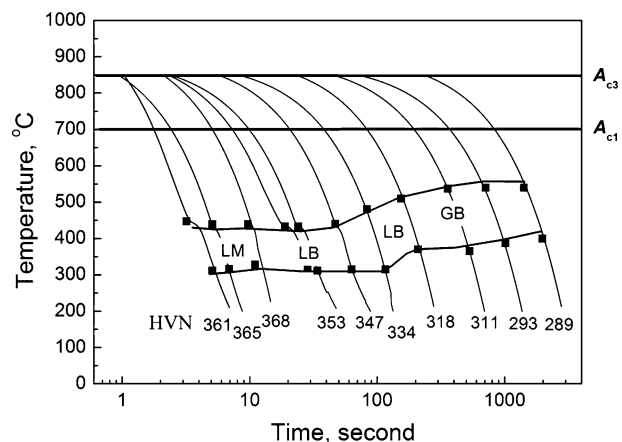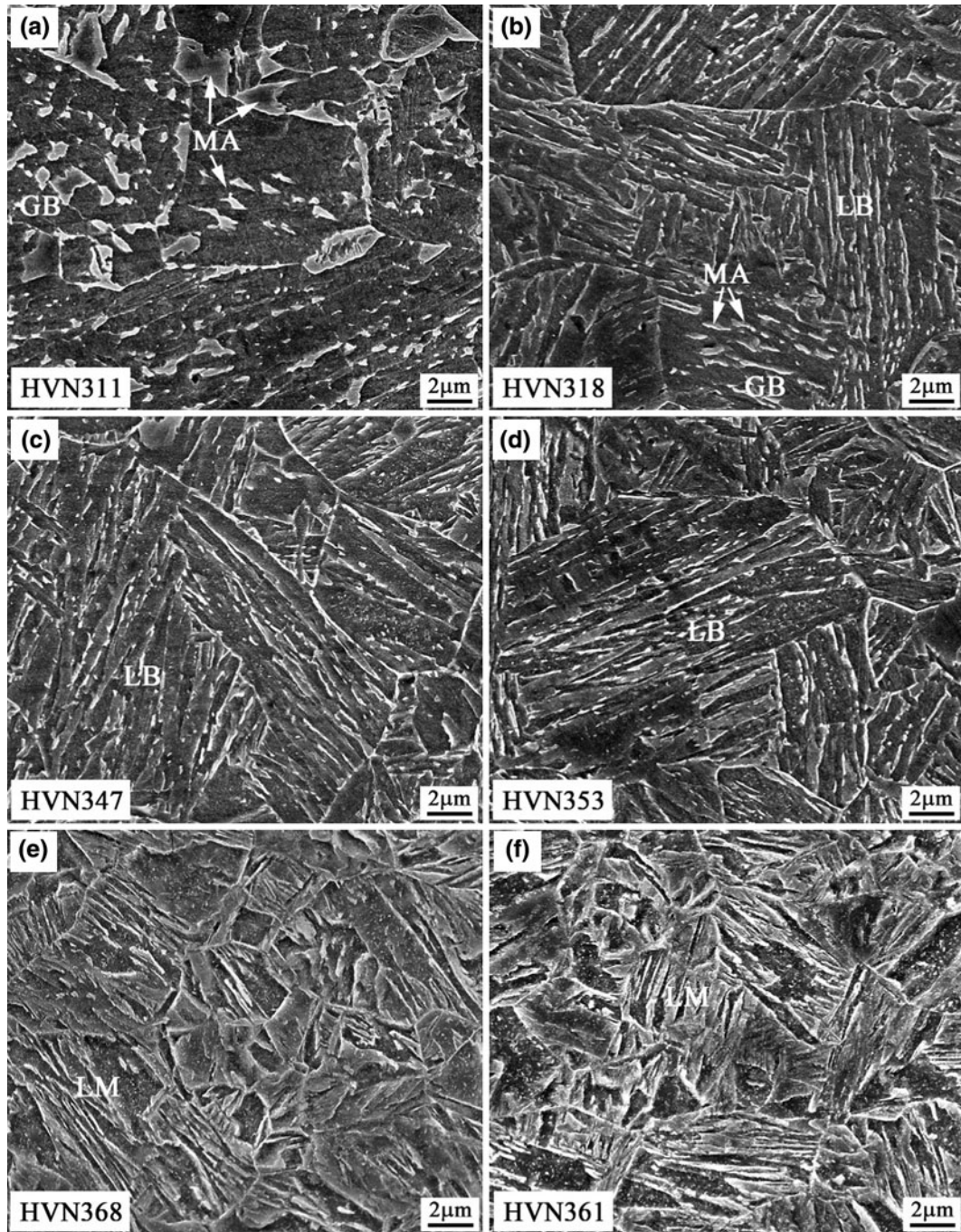

Fig. 1—CCT diagram of the current steel.

Fig. 2—SEM micrographs of the specimens cooled at (*a*) 1 K/s, (*b*) 2.5 K/s, (*c*) 10 K/s, (*d*) 20 K/s, (*e*) 50 K/s, and (*f*) 200 K/s.

leading to a HVN of 193. The microstructure is, however, fully martensitic (LM) in the HSLA-100 steel (0.04C, 0.87Mn, 1.77Cu, 3.54Ni, 0.58Cr, and 0.57Mo) cooled at the same rate.[9] A mixture of LB and LM is formed leading to the HVN of 347 in the currently investigated steel cooled at 10 K/s (10 °C/s). One can therefore conclude that the hardenability of the current steel is higher than that of the HSLA-80 steel as presented by Thompson *et al.*[18] and lower than that of the HSLA-100 steel as given by Dhua *et al.*[9] This can

be attributed to the fact that the current steel has moderate alloying level between the HSLA-80 steel and HSLA-100 steel. The variation trend of the CCT behavior is consistent with the variation of steel compositions among the three steels as mentioned.

B. *Macrostructures of the Slab and Plate*

Internal quality of the 320-mm-thick slab and the 80-mm plate (Figure 3) benefit from the production of
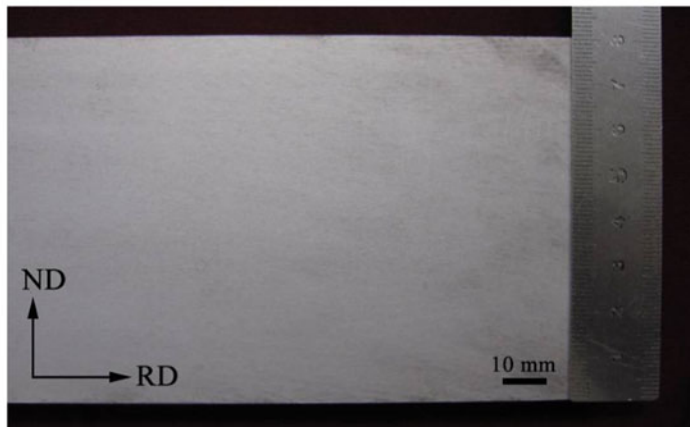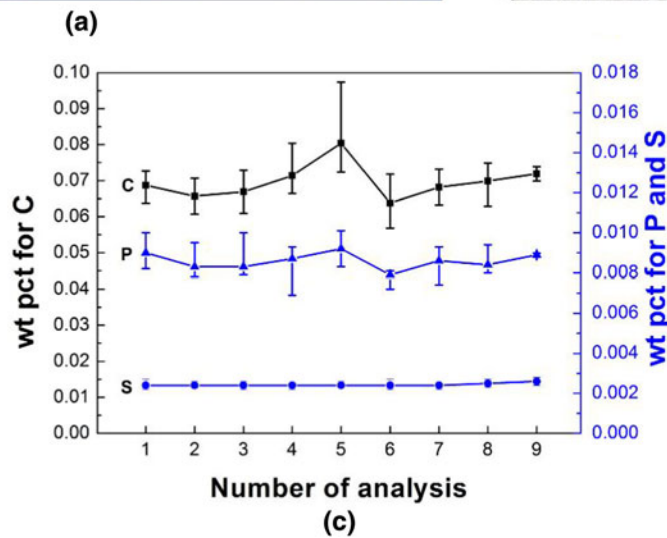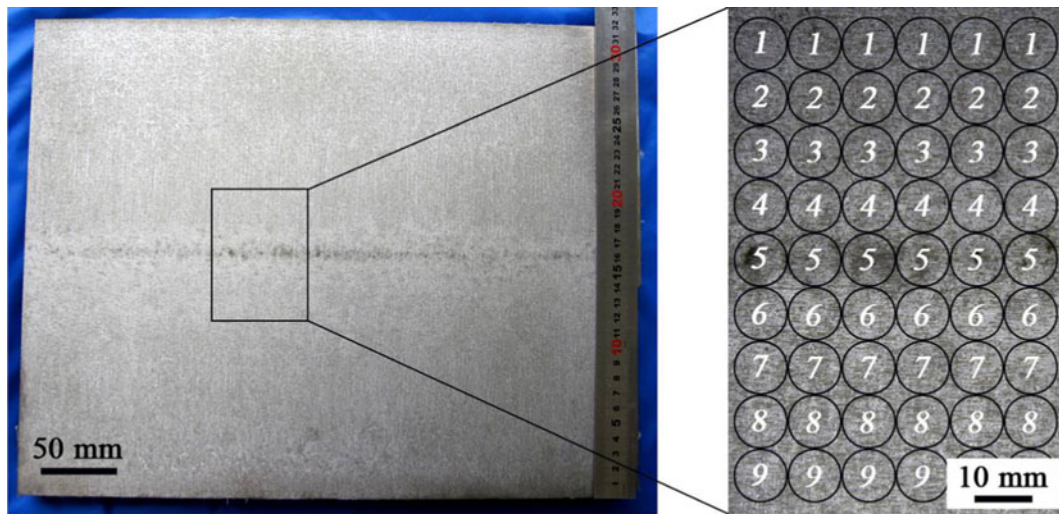
Fig. 3—Macrostructures of the slab and sample plan (*a*), location of tested area for a PDA test (*b*), distribution of chemical elements across the thickness (*c*), and macrostructure of the 80-mm-thick heavy plate (*d*).

hot metal and integrated steelmaking system consisting of basic oxygen furnace, ladle furnace, Ruhrstahl-Hereus, and continuous casting incorporating with "soft" reduction facilities. The macroetching picture of the slab (Figure 3(a)) and a center area submitted for chemical composition analysis (Figure 3(b)) employing a pulse discrimination analysis (PDA) method[19] are indicated. All alloying elements of the steel were
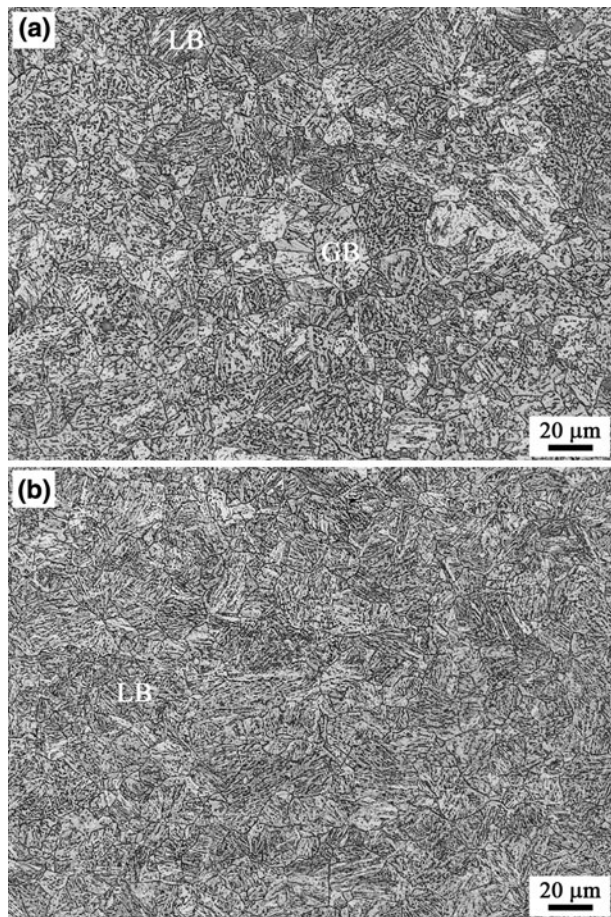
Fig. 4—OM micrographs of the as-quenched 80-mm-thick plate at (*a*) central thickness (*t*/2) and (*b*) quarter thickness (*t*/4).

quantified by the PDA method. Weak segregation of C and P (Figure 3(c)) was found and no evidence of segregation of other alloying elements was detected. The inner quality of the 80-mm-thick plate subjected to the quenching and tempering process is excellent (Figure 3(d)). Severe compositional segregation normally causes band structure in steel plates, which results in deteriorated impact toughness.[20] The homogenous structure of the current heavy plate can be attributed to the minimized level of segregation of the slab. Occurrence of band structure (if any) due to the segregation can also be suppressed under the quenching process according Majka *et al*.'s study.[21] As a matter of fact, the *Z*-direction properties were tested for the current 80-mm-thick QT-treated plate using the procedures given in Reference 14. Excellent properties in the *Z* direction (ψ_Z = 70 pct, YS = 728 MPa, ultimate tensile strength [UTS] = 790 MPa) were also observed. As a result, variation of mechanical properties along the thickness direction will be marginally attributed to the weak chemical segregation. Microstructural change along the thickness due to the difference of cooling rate during quenching will be the main factor affecting the mechanical properties of the plate.

C. *Microstructures of the As-Quenched Heavy Plate*

OM micrographs of the as-quenched heavy plates are presented in Figure 4 showing LB + GB at *t*/2 and LB at *t*/4, respectively. At *t*/2, MA constituents sized at 0.4 to 2.0 μm are associated with bainitic matrix (GB) (Figure 4(a)). The subgrain boundaries of the GB, however, cannot be identified. At *t*/4 with lathlike microstructures, several packets of LB with different orientations were produced in the same austenite grain, and the interlath (subgrain) boundaries within the same packet were also identified.

Figure 5 shows the detailed microstructures of the 80-mm-thick as-quenched plate. Laths of bainitic ferrite are major structures across the entire thickness section. The width of the laths varies from approximately 0.4 μm at *t*/2 to 0.2 μm at *t*/4. Islands of MA associated with bainitic ferrite, *i.e.*, GB were frequently observed at *t*/2, while fine MA constituents were mainly found between the laths of LB at *t*/4. Precipitation of Cu was hardly found in the bainitic grains across the thickness section of the as-quenched plate.

D. *Microstructure Evolution of the Tempered 80-mm-Thick Plate*

Figures 6 and 7 show the microstructure of the QT-treated plate tempered for 240 minutes at 723 K and 898 K (450 °C and 625 °C), respectively. Fine spherical precipitates of Cu are observed in the plate tempered at 723 K (450 °C). Twinned martensite grains are no longer found in the plate tempered at 898 K (625 °C), although the outline of LB structure is observed (Figures 7(a) and (c)). The LB grains are fragmented by the formation of quasi-polygonal ferrite (QPF) grains within the laths. Cr- and Mn-bearing carbides precipitate from the twinned martensite. The nanometer-scale Cu-bearing precipitates (Figures 7(b) and (d)) were characterized by the element-mapping technique in the tempered bainitic grains.

Figure 8 shows EBSD maps by high-angle grain boundaries (HAGBs) having a misorientation greater than 15 deg in the subject plates under the as-quenched (Figures 8(a) and (b)) and tempered (Figures 8(c) and (d)) conditions. The fraction of HAGBs as indicated is quantified based on the distribution of grain-boundary misorientations taken from each EBSD measurement. The fractions of HAGB at *t*/4 are higher than those at *t*/2. The effective grains[22–26] at *t*/2 with GBs are coarser than those at *t*/4 with LBs under both as-quenched and the QT conditions. The misorientations of initial austenite grain boundaries are inherently greater than 15 deg. The misorientations of LBs boundaries are also higher than 15 deg. However, those of subgrain-boundary of GBs are smaller than 15 deg such that the effective grains of GBs are large. It is noted that MAs associated with GB matrix of the as-quenched plate are highly dislocated and twinned as already characterized by the current TEM work. Their boundaries are HAGBs.[25]
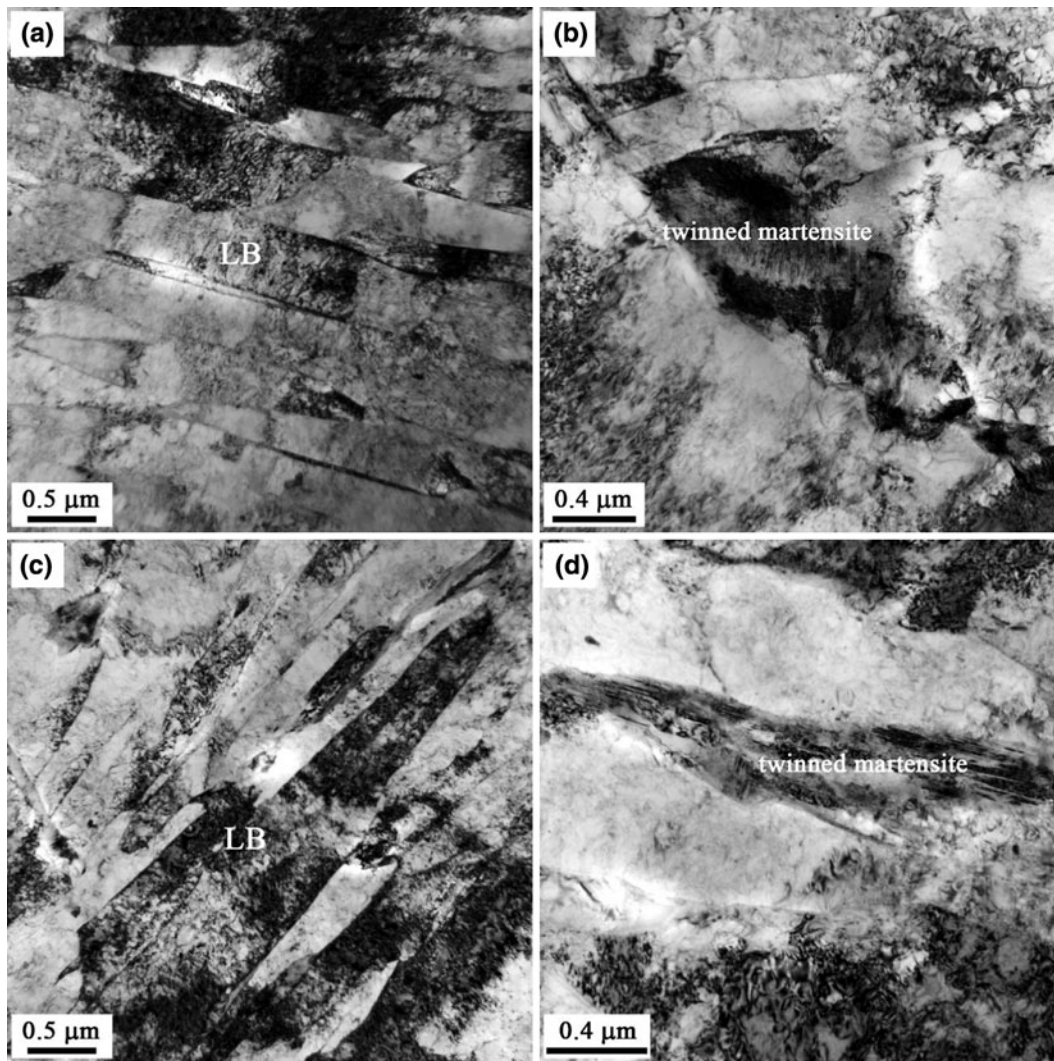
Fig. 5—TEM images of the water quenched heavy plate at (*a*) and (*b*) *t*/2, (*c*) and (*d*) *t*/4.

E. *Mechanical Properties*

The dependence of mechanical properties of the plates upon tempering was investigated. The room-temperature stress–strain curves indicate a continuous yielding behavior at the as-quenched condition and a variation trend from continuous to discontinuous yielding behavior with the increase of tempering temperature, as shown in Figure 9. Mobile dislocations formed inside the low-temperature transformation phases such as GB and LB are promoted by the hard phase of MA constituents as shown in Figure 5 leading to the continuous yielding behavior.[22,25] The pinning effect of the precipitates of Cu is anticipated in the tempered plates resulting in a lock on the dislocations. Furthermore, the promoting effect of the MA constituents on the mobile dislocations was eliminated due to tempering of the constituents at 823 K (550 °C) and above. These factors lead to the discontinuous yielding behavior of the tempered plates. Similar discontinuous yielding behavior due to precipitates of Nb(C,N) and martensite tempering were also observed and discussed by Bai *et al*.[27,28]

The variations of tensile properties (elongation [EL]), hardness (HVN), and low-temperature CVN toughness on tempering temperature are shown in Figure 10.

The as-quenched plate sample at *t*/4 with LB + LM exhibited well-balanced hardness, strength, and low-temperature toughness with a YR 0.76. In comparison, the sample at *t*/2 with GB exhibited lower hardness, strength, ductility and deteriorated CVN toughness.

The hardness, strength, CVN toughness, and elongation vary as the tempering temperature increases. The YS increases from 743 MPa (*t*/2) and 793 MPa (*t*/4) of the as-quenched plate to the highest levels of 894 MPa (*t*/2) and 947 MPa (*t*/4) on tempering at 723 K (450 °C). As the tempering temperature increases between 723 K and 948 K (450 °C and 675 °C), a continuous decrease in YS is observed, reaching minimum YS of 637 MPa (*t*/2) and 650 MPa (*t*/4). Similar variation trends upon tempering temperature are found in HVN and UTS at both *t*/2 and *t*/4. On the other hand, the low-temperature CVN toughness decreases sharply on tempering at 723 K (450 °C). The CVN toughness at *t*/2
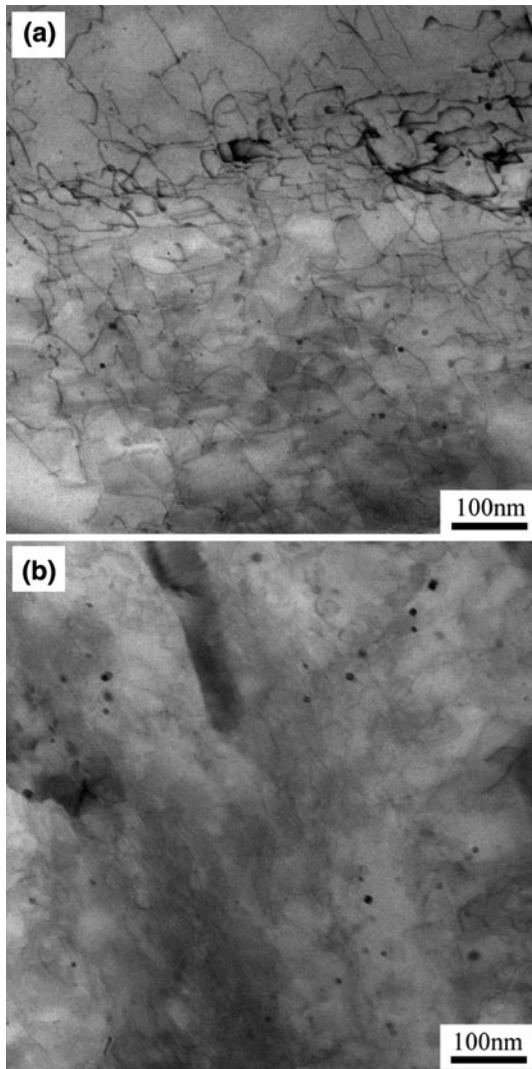
Fig. 6—TEM images of the water quenched 80-mm thick plate tempered at 723 K (450 °C) for 240 min at (*a*) *t*/2, (*b*) *t*/4, showing fine precipitates of Cu (the images were taken using scanning transmission electron microscopy).

starts to increase with the tempering temperature and attains the maximum average value at approximately 180 J even at 193 K (−80 °C) on tempering at 948 K (675 °C). Sound combination of strength (YS = 718 to 778 MPa, UTS = 778 to 791 MPa), ductility (EL = 19.8 to 23.4 pct), and low-temperature (193 K [−80 °C]) CVN toughness (approximately 150 J) was achieved across the entire thickness section of the heavy plate, which is well above the specification of NV-F690 plate for shipbuilding on tempering at 898 K (625 °C) for 240 minutes.

F. *The Impact Fracture Behavior*

The typical impact fracture course of the CVN curves consists of crack forming at the maximum impact load (P_m), crack propagation, brittle fracture at the brittle fracture start load (P_f), and postbrittle fracture starting from the fracture arrest load (P_a).[29–32] The curves of CVN impact load combined with the impact energy *vs* hammer displacement were plotted based on the data recorded by the instrumented Charpy impact machine for a series of CVN tests conducted at 193 K (−80 °C), as shown in Figure 11. The CVN toughness increases with the increase of the difference of P_m and P_f ($P_m − P_f$) and the ratio of P_m to P_a (P_m/P_a). When the as-quenched plate is tempered at 873 K (600 °C), a brittle fracture is observed on the sample at *t*/2, while ductile fracture is observed on the sample at *t*/4. The difference between $P_m − P_f$ and P_m/P_a for the sample at *t*/2 are lower than those at *t*/4. The absorbed energy at *t*/2 is associated only with the crack initiation without much energy consumed during the abrupt brittle crack propagation, while at *t*/4, both crack formation and substantial crack propagation before the brittle fracture result in high absorbed energy. When the plate is tempered at 898 K (625 °C), ductile fracture takes place on the sample either at *t*/2 or at *t*/4. The crack arrest capacity at *t*/2 is, however, lower than that at *t*/4 as indicated by the difference of P_a.

SEM fractographs of the CVN samples fractured at 193 K (−80 °C) corresponding to the curves in Figure 11 are presented in Figure 12. Figures 12(a) and (b) show quasi-cleavage fracture surface of the sample at *t*/2 and ductile fracture surface featured by dimples at *t*/4, respectively, of the plate tempered at 873 K (600 °C). The samples at both *t*/2 and *t*/4 of the plate tempered at 898 K (625 °C) exhibit dimples. The results of the fractographic study are consistent with the curves of load and CVN absorbed energy *vs* hammer displacement achieved in the instrumented impact tests.

G. *Weldability*

High-strength accompanied with high low-temperature-toughness has been achieved in the parent plate due to the sophisticated microstructures with high fractions of HAGB and Cu precipitates. The mechanical properties of the HAZs of the welded joints, however, must be reexamined because the microstructures of the plate will be altered after multipass welding procedures.

The coarse-grained HAZ (T_P^1 = 1623 K [1350 °C]) can be categorized into four zones according to the second peak temperature (T_P^2) as defined by Lee *et al*.[33,34] and de Meester[35]: (1) a subcritically reheated coarse-grained zone (SRCG HAZ), the zone reheated below A_{c1}; (2) an intercritically reheated coarse-grained zone (ICRCG HAZ), the zone reheated between A_{c1} and A_{c3}; (3) a supercritically reheated coarse-grained zone (SCRCG HAZ), the zone reheated above A_{c3}; and (4) an unaltered coarse grained-zone (UACG HAZ) the zone that is not reheated or reheated above 1423 K (1150 °C). Table III shows the effect of the second peak temperature on the hardness, CVN impact toughness of the simulated HAZs. Excellent toughness is obtained at the SCRCG HAZ, while the toughness at other HAZs cannot achieve the targets as defined for the parent NV-F690-steel plate. The latter HAZs are so called "local brittle zones" (LBZs). As the cooling rate decreases ($\Delta t_{8/3}$ = 62 seconds), the low-temperature toughness at the SCRCG HAZ generally decreases. As a result, one can speculate that excellent toughness values will be achieved even at 213 K (−60 °C) when the
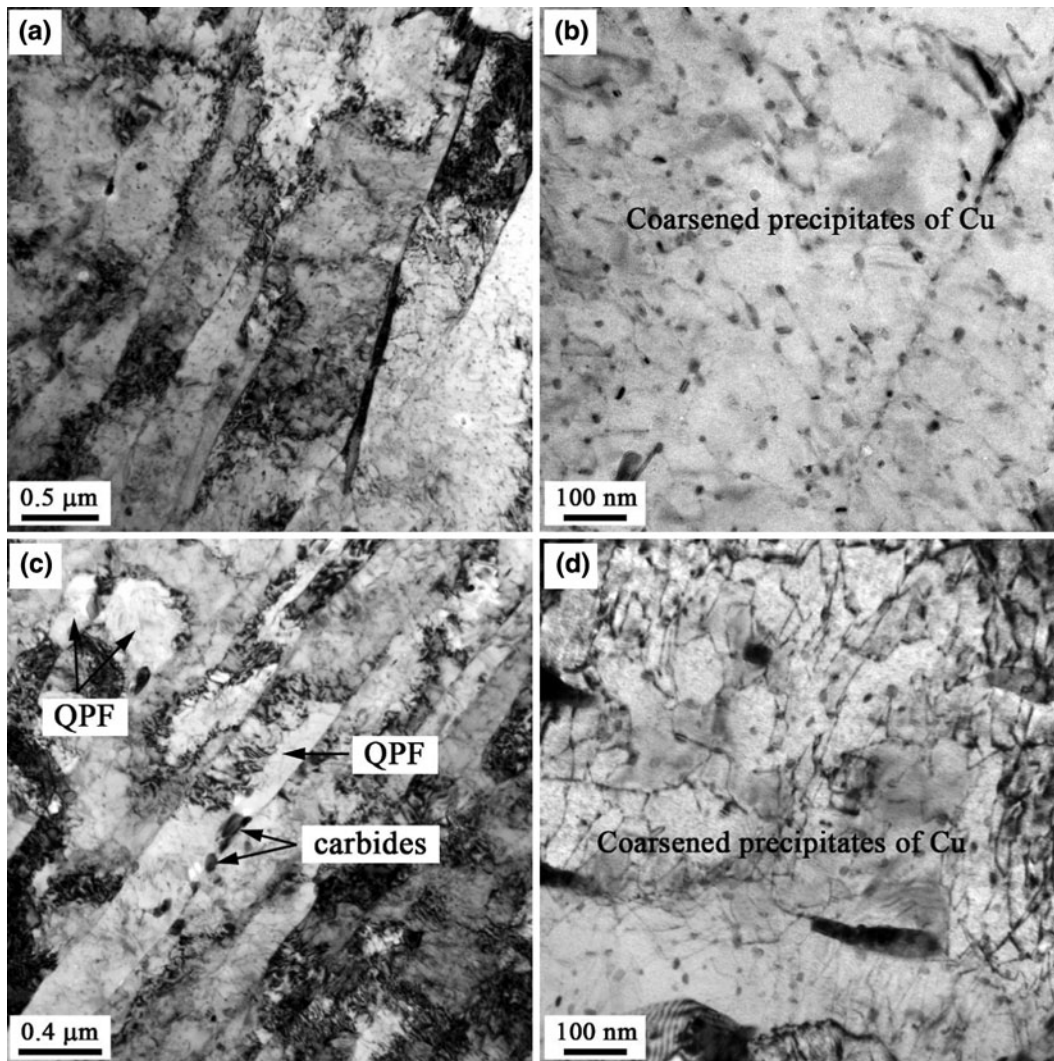
Fig. 7—TEM images of the water-quenched, 80-mm-thick plate tempered at 893 K (625 °C) for 240 min at (*a*) and (*b*) *t*/2, (*c*) and (*d*) *t*/4.

T_P^2 is ranged from 1173 K to 1373 K (900 °C to 1100 °C) with $\Delta t_{8/3}$ at 38 to 62 seconds. During multipass welding procedures, the deposition of successive beads should be done by controlled heat input to reduce the fraction of LBZ.[35]

The microstructures at different HAZ conditions are shown in Figure 13. At SCRCG HAZ where T_P^2 reaches 1223 K (950 °C) with $\Delta t_{8/3}$ at 38 seconds, the microstructure is mainly LB, which corresponds to the high HVN of 346 and best HAZ toughness at 213 K (−60 °C). The hardness is within the limit for the fabrication of offshore structures and icebreaker ships. When $\Delta t_{8/3}$ is increased to 62 seconds, the bainitic laths and M/A constituents become coarser, leading to the decreased hardness and toughness.

The current work is only restricted within the study on the effect of thermal cycles on toughness and microstructure of the simulated HAZs to find suitable welding process for the subject plate steel. More comprehensive research on the relationship of microstructure and properties of the welded joints[32–34] is essential to the future work.

IV. DISCUSSION

Advanced heavy steel plates up to 80 mm thickness with sound macrostructure across the thickness and mechanical properties comparable with conventional HSLA-100 steel plates have been developed under the integrated industrial production condition by using the steel composition much leaner than that of the HSLA-100. The characteristics of the continuously cooled microstructures of the plate and HAZs and their evolution on tempering, as well as the effect of microstructural factors on mechanical properties of the 80-mm-thick plates, are discussed as follows.

A. *Precipitation Behavior During Continuous Cooling*

The precipitation behavior in copper-bearing plate steels during continuous cooling and microstructures vary with steel composition and cooling rate. Non-Cu precipitation took place during the quenching in the current plate, which is different from the results
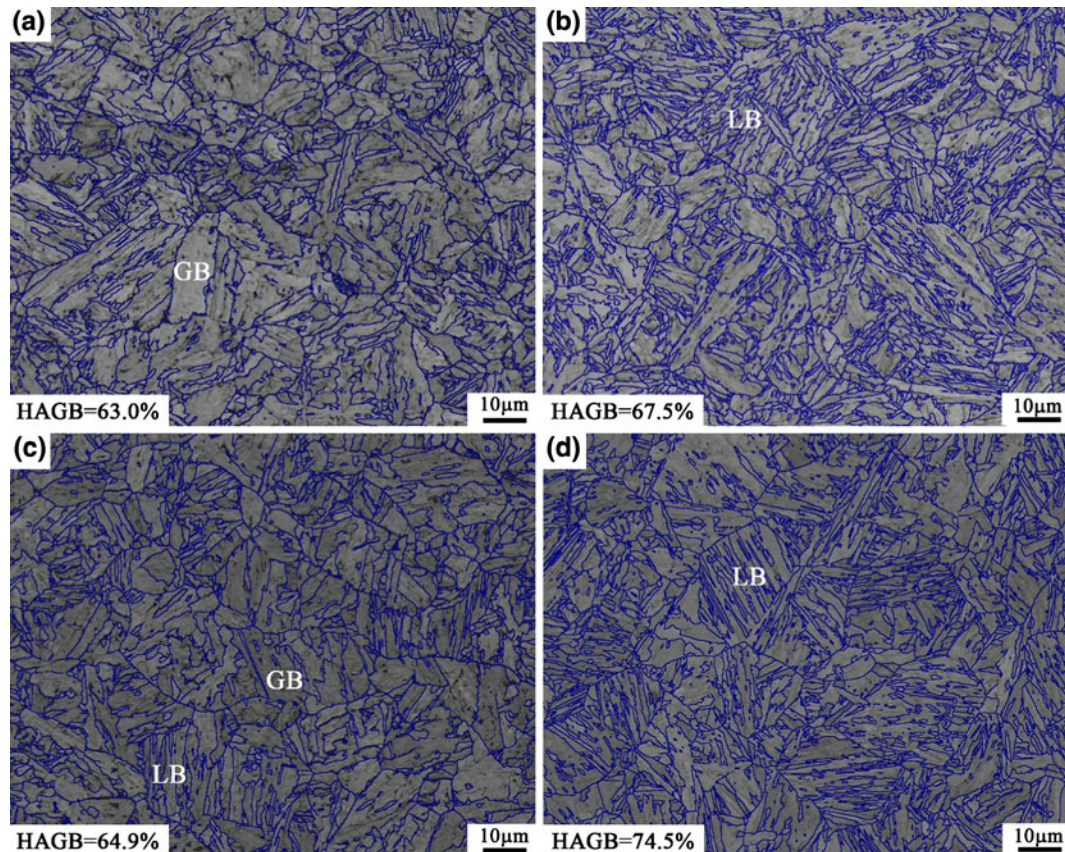
Fig. 8—Band contracts in EBSD analysis of the 80-mm-thick plate under (*a*) and (*b*) as-quenched condition, (*c*) and (*d*) water-quenched and tempered at 893 K (625 °C) for 240 min (a) and (c) *t*/2, (b) and (d) *t*/4 (thick lines indicate high-angel grain boundaries with misorientation angle greater than 15 deg).

observed in the HSLA-100 steel.[9] Dhua et al.[9] presented evidences showing Cu and Nb(C,N) precipitates in the water-quenched HSLA-100 steel with 1.77 pct Cu cooled even at 130 K/s (130 °C/s). Li et al.[36] showed, on the other hand, that Cu precipitation cannot take place during continuous cooling at 5 K/s (5 °C/s) and higher in low-carbon Fe-Cu alloys with Cu content at approximately 1.0 wt pct. Thompson and Krauss[37] showed that the copper-bearing precipitates were formed mainly by interphase mechanism in the HSLA-80 steel cooled at 10 K/s (10 °C/s), while it took place in the A710M steel (0.06C, 1.45Mn, 1.25Cu, 0.97Ni, 0.72Cr, and 0.42Mo) cooled at a much slower rate of 0.1 K/s (0.1 °C/s). The significant retardation effect of manganese and molybdenum on the precipitation can be realized based on Thompson et al.'s study. In the current work, LB and GB structures without evidences of the precipitation of Cu were produced in the 80-mm heavy steel plate after water quenching. The absence of precipitates in the as-quenched plate of the current steel can be explained by the retardation effect of the alloying elements on precipitation. This is not necessarily in conflict with Dhua et al.'s[9] finding because the content of copper in the current steel is much less than that in the HSLA-100 steel.

The Cu precipitates dissolve in austenite at peak reheat temperatures, and then the precipitation behavior of Cu during cooling depends also on chemical composition and cooling rate in the HAZs of the welds. Shome et al.[8,38] studied the transformation kinetics and microstructure of single-pass simulated HAZs in an HSLA-80 steel with Cu and Ni content similar to the current steel and found no evidence of Cu precipitation in the simulated HAZs with cooling rates higher than 12 K/s (12 °C/s). The absence of Cu precipitation can be attributed to the low Cu content and low γ to α phase transformation temperatures. Typical transformation kinetics in the HAZs is shown in Figure 14. At the low transformation start and finish temperatures, one can anticipate based on the previous studies[8,36–38] and the study on the as-quenched microstructure on the current steel that very few (if any) Cu-bearing precipitates can be formed in the current HAZs during the transformation process. The possibility to attain the maximum precipitation strengthening increment due to auto-aging is extremely low (if not impossible) at the transformation finish temperatures[5] in the simulated SCRCG and UACG HAZs. It is, however, possible that the maximum Cu precipitation strengthening
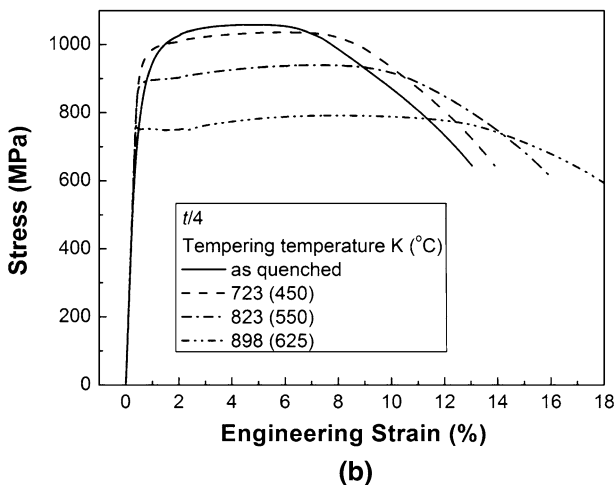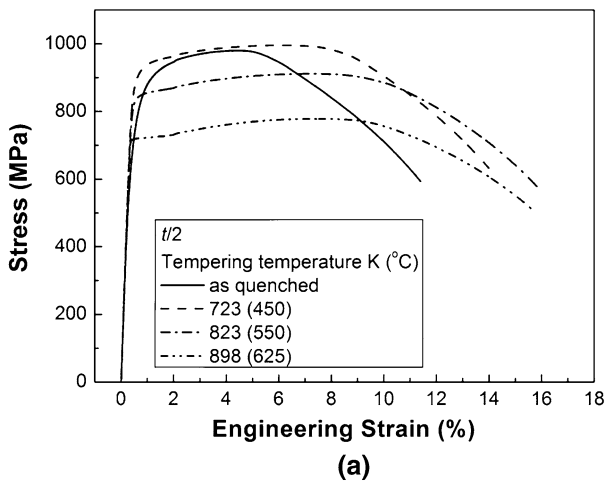
(a)

(b)

Fig. 9—Room-temperature stress–strain curves corresponding to the specimens taken from the as-quenched and tempered plates at t/2 (a), and t/4 (b).

increment is attained lending to the formation LBZs in the SRCG and ICRCG HAZs due to tempering of the coarse-grained HAZ.

B. Increased Fraction of HAGB on Tempering

It is found in the current work that the fraction of HAGB is increased after the LB is tempered. The fraction of HAGB at t/4 with LBs due to tempering is more substantially increased than that at t/2 with GBs. The TEM observations show that ferrite subgrains preferentially nucleated in the matrix of fine LBs generating new substructure boundaries, which in turn increase the fraction of HAGB of the bulk sample at t/4. The increase of HAGB decreases the effective grain size of the tempered LB structure. Gao et al.[39] investigated the effect of tempering on the toughness of a high-Mn low-carbon bainitic steel produced by hot rolling. They also found that tempering caused an increase of HAGB and hence a decrease of the effective grain size of the LB structure. However, the current study reveals for the first time that the increase of HAGB caused by

tempering is negligible when the as-quenched microstructure is GB.

C. The Relationship of Mechanical Properties and Microstructure

1. As-quenched steel

The EBSD analysis of the current work enables in-depth understanding on the relationship between microstructural factors and mechanical properties in the ultra-high-strength Cu-bearing bainitic steel. The ductile–brittle transition temperature (DBTT) strongly depends on the chemical composition, strength, effective grain size, and the fraction and size of MA constituents in martensitic and bainitic steels.[23–26] The DBTT rises with strength and effective grain size. This can explain the difference of CVN toughness at t/2 and t/4. Cleavage fracture was observed on the CNV specimens at t/2. The specimens exhibited much lower toughness than those at t/4 for two reasons. First, the coarse MA constituents worsen the CVN toughness by reducing the crack initiation energy. Second, GB is present at t/2 with a large effective grain size, which in turn increases the DBTT due to decreased resistance to crack propagation. As a result, the DBTT of the specimen at t/2 of the 80-mm-thick plate is higher than 213 K (−60 °C) leading to the predominance of cleavage fracture. The effective grain boundaries with misorientation greater than 15 deg in turn enhance the resistance to crack propagation. The effective grain size decreases as the fraction of HAGB increases leading to the decrease of DBTT. As a result, the strength and low-temperature toughness of the specimen at t/4 is higher than those of the specimens at t/2. The current investigation on the microstructures and mechanical properties of the as-quenched heavy plate enrich the databases of physical metallurgy of Cu-bearing steels. The as-quenched plate is subjected to further tempering treatment to reach decent combination of high strength and toughness.

2. As-quenched steel subjected to tempering

The tempering characteristics of copper-bearing HSLA-100 steels with LM were discussed by early studies.[1–6] The variation trend of mechanical properties of the subject bainitic steel plate upon tempering in the range of 673 K and 923 K (400 °C and 650 °C) of the current work is generally consistent with the that found in the martensitic steels as summarized by Dhua et al.[4] However, tempering characteristics are differentiated by comparing the microstructures and properties of the specimens containing LB (t/4) and GB (t/2). Tempering at 898 K (625 °C) and higher leads to significant improvement of the CVN toughness over that of the as-quenched plate at t/2. This can be attributed to two reasons. First, the softening of the bainitic grains due to the reduction of dislocation density lowers the DBTT and, hence, the low-temperature toughness.[1–4] Second, the decomposition of the coarse MA constituents into carbides eases their detrimental effect on the resistance to crack initiation toughness. The combination of strength and toughness at t/4 is superior to that at t/2 because the refinement of effective grain size at t/4 is
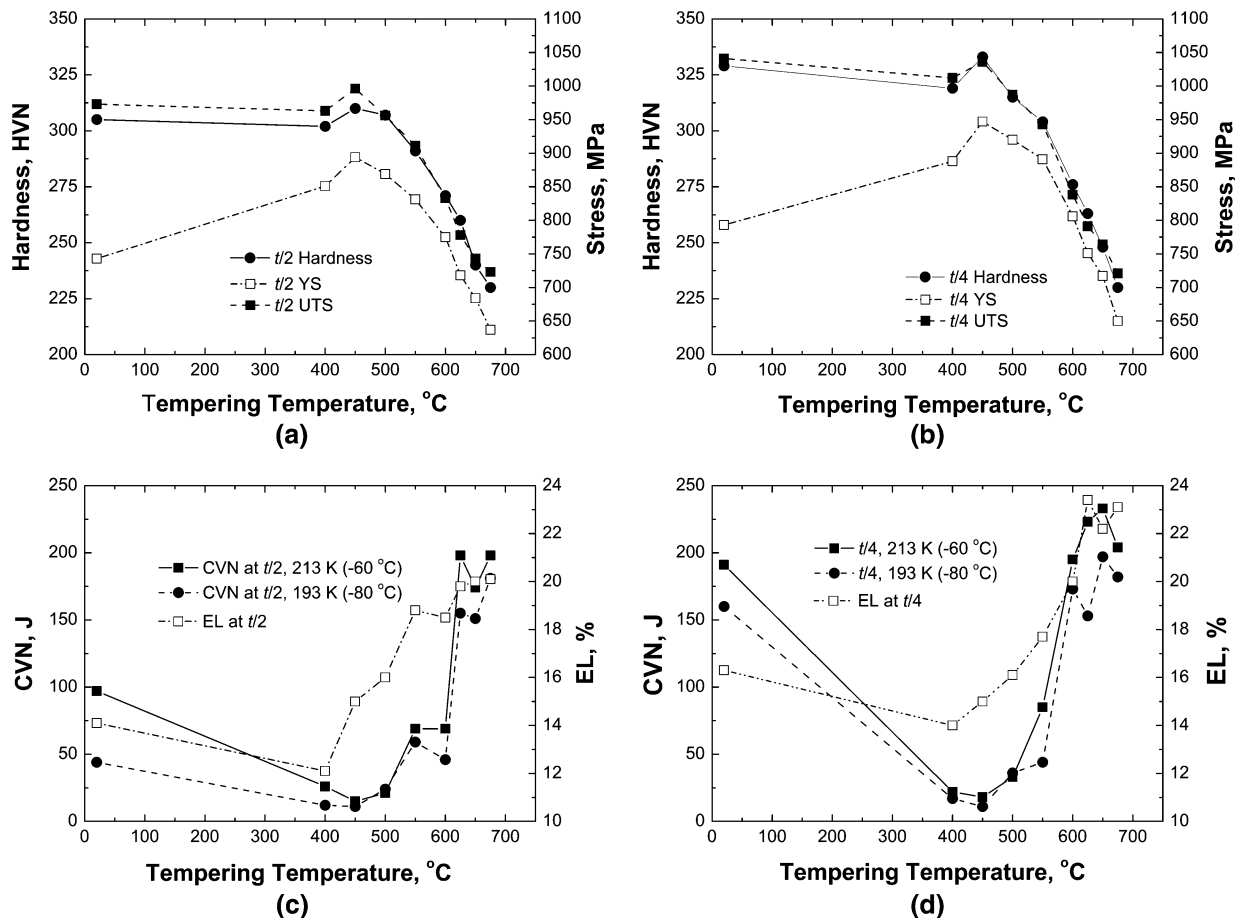
Fig. 10—Variation of mechanical properties with tempering temperature. (*a*) HVN, YS, UTS at *t*/2; (*b*) HVN, YS, UTS at *t*/4; (*c*) Charpy absorbed energy (CVN) and elongation (EL) at *t*/2; (*d*) CVN and EL at *t*/4.

more significant than that at *t*/2 according to the EBSD analysis.

Substantial quantity of precipitates of Cu are evident in the plate tempered at 898 K (625 °C), which compensates the loss of strength due to the softening of the tempered matrix, leading to the best combination of strength and toughness across the thickness section.

V. CONCLUSIONS

A systematic study has been carried out on the microstructure and mechanical properties of the advanced heavy-plate steel. The investigation is intended to bridge fundamental materials characterization and integrated industrial production, providing database for chemical composition and process parameters for commercializing the advanced high-strength plate steel. The following conclusions are made:

1. A continuous cooling transformation diagram with an austenite grain size of 10 μm is constructed to predict the as-quenched microstructure of the heavy plates. Polygonal ferrite transformation is not observed at a cooling rate greater than 0.25 K/s (0.25 °C/s). GB associated with coarse martensite-austenite constituents is produced at 0.25 K/s to 1 K/s (0.25 °C/s to 1 °C/s) between 813 K and 643 K (540 °C and 370 °C). The mixture of LB and GB is formed at 2.5 K/s to 10 K/s (2.5 °C/s to 10 °C/s). The LB is predominant at 10 K/s to 20 K/s (10 °C/s to 20 °C/s), while LM is formed at 50 K/s (50 °C/s) and higher cooling rates between 713 K and 573 K (440 °C and 300 °C).

2. Sound macrostructure is achieved in the heat-treated, 80-mm-thick heavy plate. The microstructure of the as-quenched plate, however, varies across the thickness. At quarter thickness (*t*/4) the as-quenched microstructures consist of mainly LB. Fine MA constituents exist between the laths. At center thickness (*t*/2), the as-quenched microstructures consist of GB + LB. The fraction of HAGB at *t*/4 is greater than that at *t*/2. Cu-bearing precipitates are not observed in the as-quenched microstructures.

3. The fine and spherical particles are Cu riched in the plate tempered at 723 K (450 °C). These are coarsened in the plate tempered at 898 K (625 °C). The
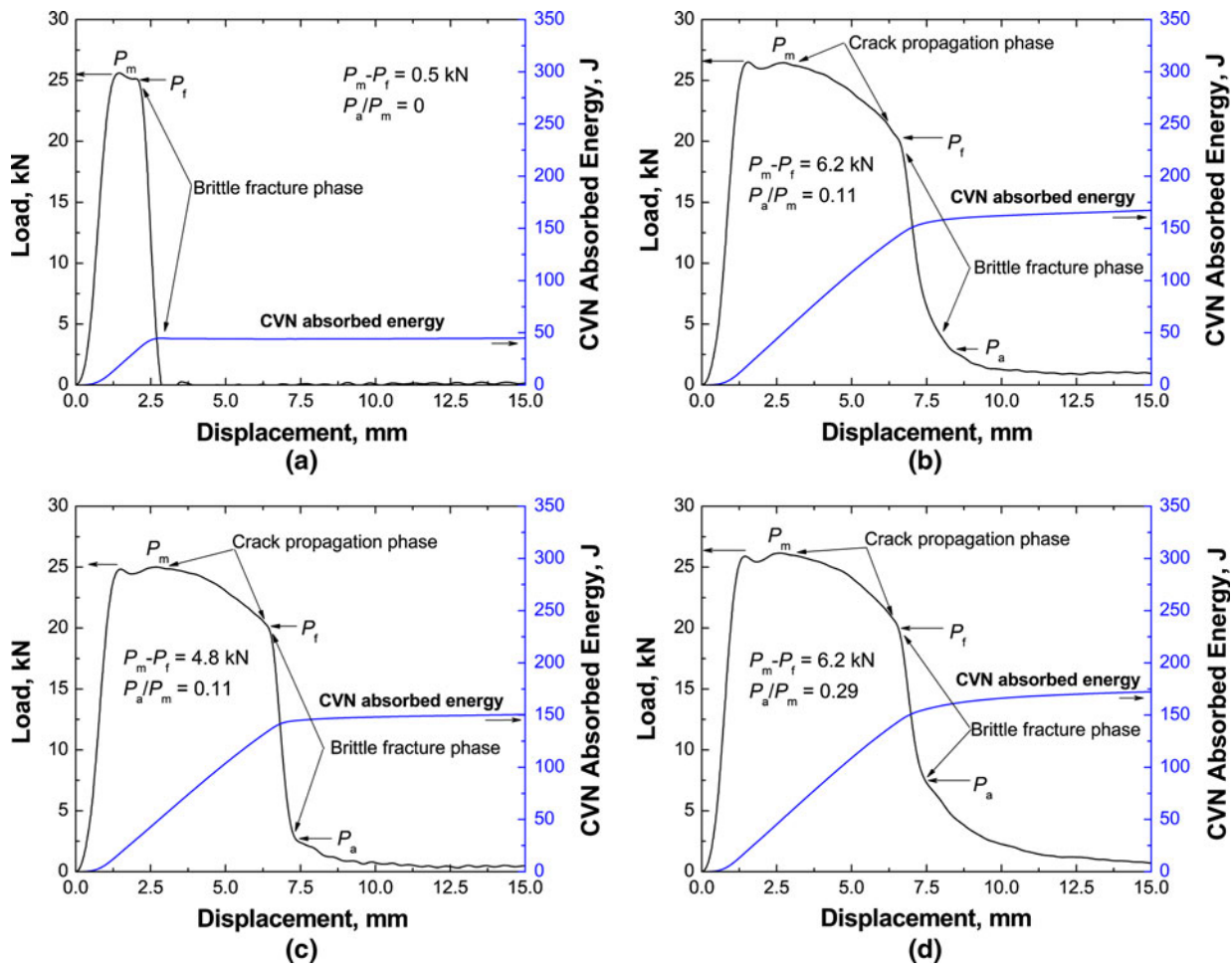
Fig. 11—Curves of load and Charpy impact energy (CVN) *vs* hammer displacement obtained in the instrumented impact tests conducted at 193 K (−80 °C) on the specimens of the water-quenched, 80-mm-thick plate tempered for 240 min at (*a*) and (*b*) 873 K (600 °C), (*c*) and (*d*) 893 K (625 °C). (a) and (c) *t*/2, (b) and (d) *t*/4.

nucleation of quasi-polygonal ferrite grains in the LB during tempering generates interfaces with large misorientation to the matrix. As a result, the fraction of HAGB is increased in the tempered LB structure. The increased fraction of HAGB is, however, negligible when the as-quenched structure is granular bainite.

4. The strengths, ductility, and low-temperature toughness at *t*/4 of the as-quenched plate with LB structure are generally good showing ductile impact fracture even at 193 K (−80 °C). However, the strengths and low-temperature toughness at *t*/2 containing GB structure are generally lower than those of *t*/4 exhibiting brittle fracture at 193 K (−80 °C).

5. Tempering at 723 K (450 °C) is found to make the highest hardness and strengths accompanied with the lowest Charpy impact toughness at either *t*/2 or *t*/4. The best combination of strength and toughness

is achieved in the 80-mm-thick plate tempered at 898 K (625 °C) for 240 minutes. Ductile fracture behavior is observed even at 193 K (−80 °C) at both *t*/2 and *t*/4. The strengths and impact toughness at *t*/4 are better than that at *t*/2 due to the predominance of finer LB and higher fraction of HAGB.

6. The toughness of the supercritically reheated coarse-grained zone is excellent achieving the target properties for the NV-F690 plate. It is also found that the unaltered coarse-grained zone, and these subjected to subcritically reheating and intercritically reheating are LBZs.

7. Heavy plates of 80-mm thickness with yield strength greater than 690 MPa and secured toughness even at 193 K (−80 °C) can be produced using the low-carbon, Cu-bearing alloy steel with alloying contents substantially lower than those of the HSLA-100 steel.
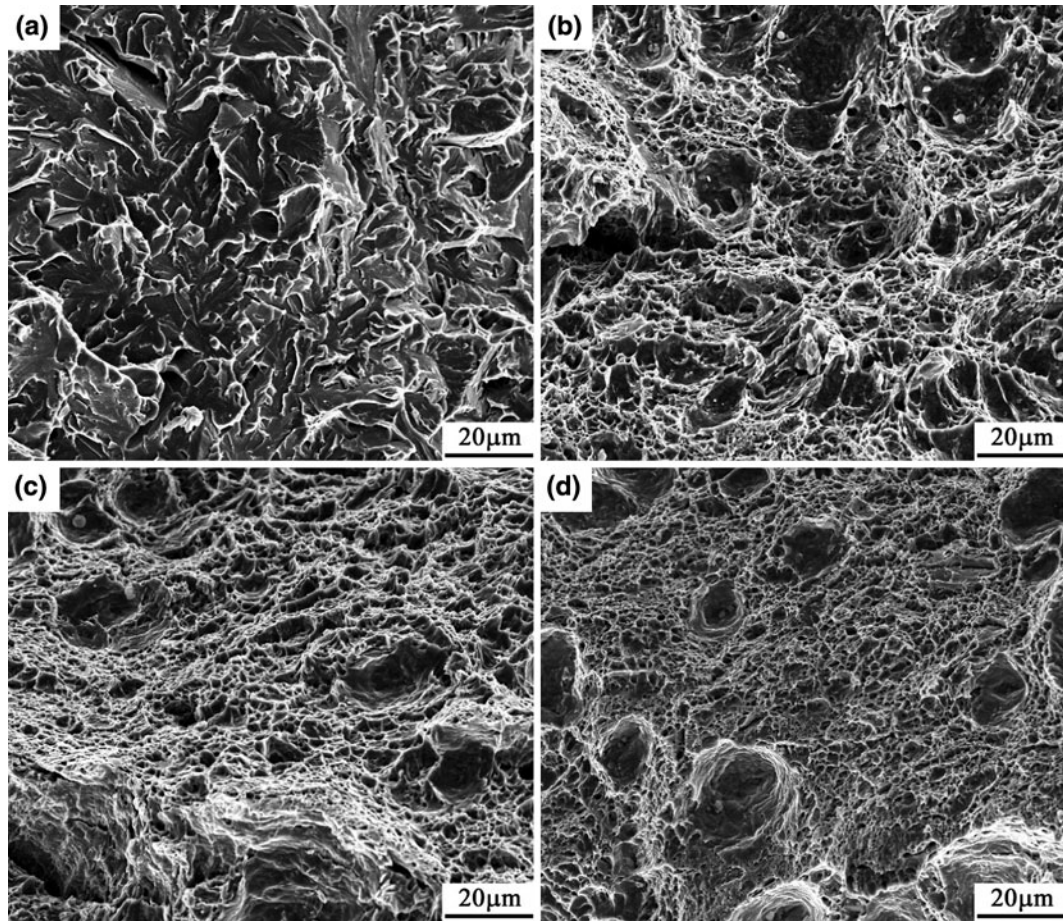
Fig. 12—SEM image of fractographs of the Charpy impact specimens fractured at 193 K (−80 °C) of the water-quenched 80-mm thick plate tempered for 240 min at (a) and (b) 873 K (600 °C), (c) and (d) 893 K (625 °C). (a) and (c) t/2, (b) and (d) t/4.

Table III. Impact Toughness at 213 K (−60 °C) in the Simulated HAZ Conditions

| T_p^1 [K (°C)]	T_p^2 [K (°C)]	$\Delta t_{8/3}$, s	Charpy Absorbed Energy (J)
1623 (1350)	—	38	40, 15, 22 (26)
	1473 (1200)		50, 39, 93 (61)
	1423 (1150)		71, 64, 81 (72)
	1323 (1050)		184, 187, 207 (193)
	1223 (950)		295, 277, 316 (296)
	1173 (900)		103, 98, 109 (107)
	1073 (800)		50, 21, 31 (34)
	1023 (750)		32, 19, 13 (21)
	873 (600)		26, 29, 43 (33)
	1423 (1150)	62	72, 78, 40 (63)
	1373 (1100)		104, 72, 83 (86)
	1323 (1050)		114, 104, 126 (115)
	1273 (1000)		107, 120, 55 (94)
	1223 (950)		94, 103, 119 (105)
	1173 (900)		179, 148, 159 (162)

Fig. 13—The effect of cooling rate ($\Delta t_{8/3}$) on microstructures in the supercritically reheated coarse-grained zone corresponding to T_p^2 equal to 1223 K (950 °C). (a) $\Delta t_{8/3}$ = 38 s and (b) 62 s.
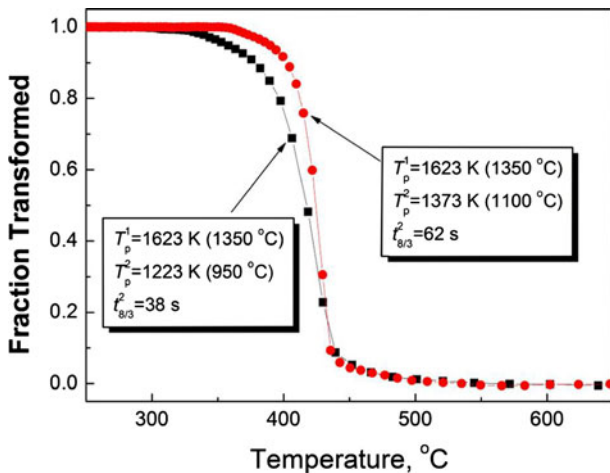

Fig. 14—CCT curves of the current steel in the supercritically reheated coarse-grained zone (SCRCG HAZ).

REFERENCES

1. A.J. DeArdo: *ISIJ Int.*, 1995, vol. 35, pp. 946–54.
2. M. Mujahid, A.K. Lis, C.I. Garcia, and A.J. DeArdo: *J. Mater. Eng. Perform.*, 1998, vol. 7, pp. 247–57.
3. G.C. Hwang, S. Lee, J.Y. Yoo, and W.Y. Choo: *Mater. Sci. Eng. A*, 1998, vol. A252, pp. 256–68.
4. S.K. Dhua, D. Mukerjee, and D.S. Sarma: *Metall. Mater. Trans. A*, 2001, vol. 32A, pp. 2259–70.
5. A.N. Bhagat, S.K. Pabi, S. Ranganathan, and O.N. Mohanty: *ISIJ Int.*, 2004, vol. 44, pp. 115–22.
6. A. Ghosh, S. Das, and S. Chatterjee: *Mater. Sci. Eng. A*, 2008, vol. A486, pp. 152–57.
7. K. Banerjee and U.K. Chatterjee: *Metall. Mater. Trans. A*, 2003, vol. 34A, pp. 1297–1309.
8. M. Shome and O.N. Mohanty: *Metall. Mater. Trans. A*, 2006, vol. 37A, pp. 2159–69.
9. S.K. Dhua, D. Mukerjee, and D.S. Sarma: *Metall. Mater. Trans. A*, 2003, vol. 34A, pp. 2493–2504.
10. D. Liu, B. Cheng, and M Luo: *Trans. Mater. Heat Treat.*, 2011, vol. 32 (9), pp. 125–35.
11. P. Hodnik, C. Fürst, P. Pennerstorfer, and H. Lengauer: *Stahl Eisen*, 2008, vol. 128 (10), pp. 35–42.
12. D. Schmidt, R. Dehmel, and G. Horn: *Stahl Eisen*, 2008, vol. 128 (8), pp. 25–30.
13. N. Shikanai, S. Mitao, and S. Endo: *JFE Tech. Report*, 2008, no. 1, pp. 1–6.
14. D. Liu, Q. Li, and T. Emi: *Metall. Mater. Trans. A*, 2011, vol. 42A, pp. 1349–61.
15. S.H. Mousava Anijdan and S. Yue: *Metall. Mater. Trans. A*, 2012, vol. 43A, pp. 1140–62.
16. D. Liu, F. Fazeli, M. Militzer, and W.J. Poole: *Metall. Mater. Trans. A*, 2007, vol. 38A, pp. 894–909.
17. V. Colla, M. Desanctis, A. Dimatteo, G. Lovicu, and R. Valentini: *Metall. Mater. Trans. A*, 2011, vol. 42A, pp. 2781–93.
18. S.W. Thompson, D.J. Colvin, and G. Krauss: *Metall. Mater. Trans. A*, 1996, vol. 27A, pp. 1557–71.
19. H. Preßlinger, S. Ilie, P. Reisinger, A. Schiefermüller, A. Pissenberger, E. Parteder, and C. Bernhard: *ISIJ Int.*, 2006, vol. 46, pp. 1845–51.
20. S.Y. Shin, S. Hong, J-H. Bae, K. Kim, and S. Lee: *Metall. Mater. Trans. A*, 2009, vol. 40A, pp. 2333–49.
21. T.F. Majka, D.K. Matlock, and G. Krauss: *Metall. Mater. Trans. A*, 2002, vol. 33A, pp. 1627–37.
22. H.K. Sung, S.Y. Shin, B. Hwang, C.G. Lee, N.J. Kim, and S. Lee: *Metall. Mater. Trans. A*, 2011, vol. 42A, pp. 1827–35.
23. B. Hwang, C.G. Lee, and T.H. Lee: *Metall. Mater. Trans. A*, 2010, vol. 41A, pp. 85–96.
24. S.Y. Han, S.Y. Shin, C.H. Seo, H. Lee, J.H. Bae, K. Kim, S. Lee, and N.J. Kim: *Metall. Mater. Trans. A*, 2009, vol. 40A, pp. 1851–62.
25. S.Y. Han, S.Y. Shin, S. Lee, N.J. Kim, J.H. Bae, and K. Kim: *Metall. Mater. Trans. A*, 2010, vol. 41A, pp. 329–40.
26. J.W. Morris, Jr.: *ISIJ Int.*, 2011, vol. 51, pp. 1569–75.
27. D.Q. Bai, T. Nelson, R. Bodnar, M. Cooke, and S. Scumpu: *Iron Steel Technol.*, 2009, vol. 6 (10), pp. 65–74.
28. D.Q. Bai, F. Hamad, J. Asante, and S.S. Hansen: *Proceedings of Microalloying for New Steel Processes and Applications*, J.M. Rodriguez-lbabe, L. Gutiérrez, B. López, and A. lza-Mendia, eds., 2005, pp. 481–88.
29. C.S. Wiesner: *Int. J. Pres. Ves. Pip.*, 1996, vol. 69, pp. 185–96.
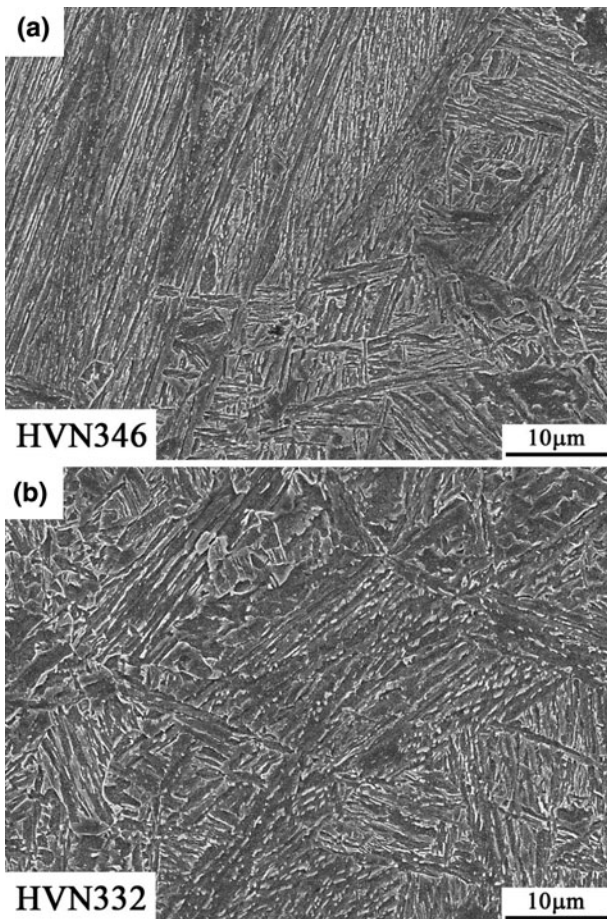
30. S.H. Hashemi: *Int. J. Pres. Ves. Pip.*, 2008, vol. 85, pp. 879–84.
31. W. Deng, X. Gao, X. Qin, D. Zhao, L. Du, and G. Wang: *Acta Metall. Sin.*, 2010, vol. 46, pp. 533–40.
32. D. Liu, B. Cheng, and M. Luo: *Acta Metall. Sin.*, 2011, vol. 47, pp. 1233–40.
33. S. Lee, B.C. Kim, and D. Kwon: *Metall. Trans. A*, 1992, vol. 23A, pp. 2803–16.
34. S. Lee, B.C. Kim, and D. Kwon: *Metall. Trans. A*, 1993, vol. 24A, pp. 1133–41.
35. B. de Meester: *ISIJ Int.*, 1997, vol. 37, pp. 537–51.
36. C. Li, X. Wang, C. Shang, C. Zheng, and X. He: *Acta Metall. Sin.*, 2010, vol. 46, pp. 1488–94.
37. S.W. Thompson and G. Krauss: *Metall. Mater. Trans. A*, 1996, vol. 27A, pp. 1573–88.
38. M. Shome, O.P. Gupta, and O.N. Mohanty: *Metall. Mater. Trans. A*, 2004, vol. 35A, pp. 985–96.
39. G. Gao, H. Zhang, and B. Bai: *Acta Metall. Sin.*, 2011, vol. 47, pp. 513–19.